Magnetic properties of electrodeposited, melt-quenched, and liquid Ni-P alloys

I. Bakonyi
Research Institute for Solid State Physics of the Hungarian Academy of Sciences, H-1525 Budapest, P.O. Box 49, Hungary

A. Burgstaller, W. Socher, and J. Voitländer
Institut für Physikalische Chemie, Universität München, Sophienstrasse 11, D-8000 München 2, Federal Republic of Germany

E. Tóth-Kádár and A. Lovas
Research Institute for Solid State Physics of the Hungarian Academy of Sciences, H-1525 Budapest, P.O. Box 49, Hungary

H. Ebert
Siemens AG, Research Laboratories, ZFE BT MR 11, Paul-Gossen-Strasse 100, D-8520 Erlangen, Federal Republic of Germany

E. Wachtel* and N. Willmann
Max-Planck-Institut für Metallforschung, Institut für Werkstoffwissenschaft, Seestrasse 92, D-7000 Stuttgart 1, Federal Republic of Germany

H. H. Liebermann
Allied-Signal Corporation, Metglas Products Department, Parsippany, New Jersey 07054
(Received 9 September 1992; revised manuscript received 17 February 1993)

A comprehensive study of the magnetic properties of $Ni_{100-x}P_x$ alloys prepared by electrodeposition with $11.5 \leq x \leq 23.2$ and by melt quenching with $16.3 \leq x \leq 21.0$ was performed for temperatures $4.2 \lesssim T \leq 300$ K in magnetic fields up to $H = 9$ kOe and, for most of the melt-quenched alloys, for $T \geq 300$ K including the molten state as well. The individual contributions to the magnetization were identified and determined separately. The matrix of Ni-P alloys was found to exhibit Pauli paramagnetism for $x \gtrsim 17$ and very weak itinerant ferromagnetism for $x \lesssim 14$. However, magnetic inhomogeneities in the form of ferromagnetic precipitates, giant-moment paramagnetic clusters and/or superparamagnetic particles could be identified throughout the whole concentration range studied and their amount and character varied significantly with alloy composition and preparation technique. In the paramagnetic phase, the temperature-independent Pauli susceptibility was not sensitive to the way of preparation, it agreed well with extrapolated room-temperature liquid-state data, decreased approximately linearly with increasing P content and extrapolated to the corresponding value of the crystalline stoichiometric compound Ni_3P. In the ferromagnetic phase, the magnetization data of the matrix could be reasonably well accounted for in terms of the Stoner-Edwards-Wohlfarth model and the theory of Mathon, yielding 85.7 at. % Ni as the critical concentration for the onset of spontaneous magnetic order. For alloys in the intermediate composition range ($14 \lesssim x \lesssim 17$), the observed magnetization was dominated by the contribution of superparamagnetic particles.

I. INTRODUCTION

It was revealed by early magnetization studies of Ni-P alloys that, similarly to other *sp* elements,[1] phosphorus reduces strongly both the spontaneous magnetization and the Curie temperature of Ni,[2] and the crystalline Ni_3P compound exhibits Pauli paramagnetism.[3] It turned out from subsequent investigations[4–8] that the transition from the ferromagnetic (FM) to the paramagnetic (PM) phase occurs in the vicinity of 15 at. % P and it has an inhomogeneous character as it is typical for Ni-based alloys.[9,10] An understanding of the nature of this FM-PM transition is further complicated by the fact that in Ni-P alloys also the atomic structure changes with increasing P content from a fcc-like Ni(P) solid solution to an amorphous Ni-P alloy phase. This structural change upon alloying occurs in the composition range from 10 to 15 at. % P.[11,12]

Previous magnetization measurements[4,5,8] on $Ni_{100-x}P_x$ alloys with $10 \lesssim x \lesssim 25$ suggest that two regimes of magnetic behavior exist. Above a critical concentration x_c which is in the middle of the composition range studied the magnetization isotherms are linear in sufficiently high magnetic fields and for not too low temperatures. In this concentration range, the alloys have a completely amorphous structure and possess no bulk

magnetic order. The magnetic behavior in this paramagnetic regime can be best described by the picture proposed by Amamou and Durand[10] for amorphous Ni-P-B alloys: the magnetization can be separated into (i) a small ferromagnetic term attributable to crystalline Ni or Ni(P,B) precipitates and (ii) a paramagnetic contribution of the amorphous matrix. The PM contribution can be further subdivided into two contributions.[10] The first term can be described by a Curie-Weiss- (CW) type susceptibility due to giant-moment PM clusters consisting of Ni-rich segregations with a magnetic moment typically $5\mu_B$ to $10\mu_B$. The second term is a practically temperature-independent susceptibility χ_{nm} due to nonmagnetic atoms in the amorphous matrix which is dominated by the Pauli paramagnetism of conduction electrons.

The magnetic behavior below x_c is characterized by the occurrence of strongly nonlinear magnetic isotherms at most temperatures which become linear at very high magnetic fields ($H \gtrsim 25$ kOe) only.[5] The magnetization data of $Ni_{100-x}P_x$ alloys for $x < x_c$ have usually been analyzed[4,5] with the help of Arrott plots in terms of weak itinerant ferromagnetism (WIF). The same approach has been applied for an amorphous $Ni_{81.6}B_{18.4}$ alloy[13] exhibiting similar magnetic behavior. However, since magnetization,[7,8,14] nuclear magnetic resonance,[7,14] and small-angle X-ray scattering[8] studies of amorphous Ni-P and Ni-B alloys have already indicated the presence of superparamagnetic particles in these systems around the PM-FM transition, it seems to be necessary to analyze the magnetization data by considering a superparamagnetic contribution as well.

In the present paper, a detailed magnetization study of $Ni_{100-x}P_x$ alloys prepared by electrodeposition (ED) with $11 \lesssim x \lesssim 23$ and melt quenching (MQ) with $17 \lesssim x \leq 21$ will be described and liquid-state susceptibility data for $17 \lesssim x \leq 21.0$ will also be reported. The aim of our work was (i) to get Pauli susceptibility data for ED and liquid Ni-P alloys which have not yet been available as well as to get more data for the MQ alloys and to compare results for the amorphous (ED and MQ alloys) and liquid states; (ii) to identify the critical concentration x_c separating the two magnetic regimes on properly characterized, homogeneous Ni-P alloys and to see if x_c depends on the preparation technique; and (iii) to establish the nature of the magnetic behavior for $x < x_c$ as to whether it can be ascribed to a WIF matrix or to superparamagnetic particles.

It was found that, irrespectively of the way of preparation, a homogeneous $Ni_{100-x}P_x$ matrix with $x \gtrsim 17$ exhibits Pauli paramagnetism characterized by a practically temperature-independent susceptibility whereas for $11.5 < x \lesssim 14$, it shows very weak itinerant ferromagnetism which could be described by the customary band model. However, magnetic inhomogeneities were shown to exist throughout the whole concentration range studied and their amount and character changed progressively with composition and depended significantly on the preparation technique. On the other hand, it was found that in the PM amorphous phase, the conduction electron susceptibility did not show any dependence on the preparation technique and agreed well even with the liquid-state data if these latter were extrapolated to room temperature.

The paper is organized as follows. Section II gives the details of the sample preparation and the magnetic measurements. The temperature dependence of magnetic properties and their analysis is presented in Sec. III. In Sec. IV the concentration dependence of the magnetic parameters and the characteristics of the magnetic inhomogeneities are discussed. Section V contains a summary of the conclusions derived from the present study.

II. EXPERIMENTAL DETAILS

A. Preparation and characterization of electrodeposited alloys

The ED Ni-P alloys were prepared in Budapest by an ED process described elsewhere[15] onto copper foil substrates in the form of 70-mm-diam disks with thicknesses ranging from 2 to 100 μm. The copper substrates were then chemically dissolved from the Ni-P deposits. An Auger analysis showed[15] that these ED Ni-P alloys were not contaminated by impurities.

The lateral composition homogeneity was tested on a scale of about 1 mm by measuring the thermoelectric power (TEP) since the TEP depends sensitively on the composition of Ni-P alloys and is not sensitive to the preparation technique.[15–17] Based on these investigations, it was found that a central circular part with a radius of about 10 mm had a composition inhomogeneity of at most some tenths of at. % P and this part of the disks was used for the magnetic measurements.

Three series of ED $Ni_{100-x}P_x$ alloys were produced and alloy composition was varied from 11.5 to 23.2 at. % P by changing the H_3PO_3 content (between 25 and 40 g/l) of a Brenner-type bath[15] and the deposition current density (between 10 and 50 A/dm^2). The actual P contents used for the ED Ni-P alloys are those obtained at the disk centers from the TEP versus composition relation[15,16] which was previously determined by spectrophotometric measurements. The magnetic properties have been studied for 15 different ED Ni-P alloy samples and our previous results[7] on two further ED alloys ($x = 19$ and 22) will also be included.

An x-ray diffraction investigation of the ED alloys showed a single first peak the width of which increased continuously with increasing P content. In agreement with previous studies,[11,12] the peak width increased only slightly for small and high P contents and rather rapidly at intermediate compositions. In our case, the rapid increase (by a factor of 2 to 3) of the width of the first diffraction peak occurred in the composition range $12 \lesssim x \lesssim 15$. The increase of the peak width with P content corresponds to a decrease of the effective crystallite size[11,12,18] and for $x \gtrsim 15$, ED $Ni_{100-x}P_x$ alloys can be considered as fully amorphous. Whereas for low P contents ($x \lesssim 10$) these alloys are fully crystalline,[11,12] for intermediate compositions they consist of a mixture of an amorphous and a crystalline phase and the ratio of these phases changes continuously with P content.[12]

B. Preparation and characterization of melt-quenched alloys

A melt-spinning process was used to prepare MQ $Ni_{100-x}P_x$ alloys with $16.3 \leq x \leq 21.0$ either at Allied-Signal or in Budapest in the form of 1- to 2-mm-wide and 10- to 20-μm-thick ribbons. Most of them were analyzed for composition by several techniques[16] and the compositions used here are those derived from their TEP data.[16] According to x-ray diffraction studies, all these MQ Ni-P alloys were fully amorphous, except the alloy with $x = 16.3$ which contained a considerable amount of crystalline precipitates manifested also in the temperature coefficient of electrical resistivity[19] and in the magnetic properties (see Sec. III A).

The magnetic properties have been studied for ten different MQ Ni-P alloy samples and our previous results on two further MQ Ni-P alloys (with $x = 20.2$ from Ref. 7 and with $x = 20.9$ from Ref. 20) will also be included. [The latter alloy ($x = 20.9$) is identical with the binary amorphous Ni-P ribbon of the MQ Ni-B-P alloy series;[20] however, based on our recent experience with P-content analysis,[16] the value $x = 20.9$ seems to be more reliable for this alloy, supported also by the liquid-state susceptibility data in this composition range.]

C. Measurement of magnetic properties

A Faraday-type magnetic balance was used to study the magnetic properties from room temperature down to the liquid-helium range for the ED alloys and for the MQ alloys prepared in Budapest, by measuring the magnetization isotherms at several temperatures in magnetic fields from $H = 1$ to 9 kOe in steps of 1 kOe.

For most of the MQ alloys, the magnetic properties were also measured by another Faraday balance from room temperature up into the molten state. First, the magnetization isotherms were measured at room temperature from $H = 6$ to 17 kOe and then the magnetic susceptibility χ_H was recorded continuously at $H = 17$ kOe from $T = 300$ to 1500 K at a heating rate of 5 K/min. The general shape of the χ_H vs T curves was very similar to those reported recently for a Ni-B-P alloy series.[20] Around 600 K, a large susceptibility peak was observed due to the precipitation of ferromagnetic nickel during the amorphous-to-crystalline transition.[21] The magnetic susceptibility was measured also in the liquid state at $H = 17$ kOe with 5 K/min upon heating up to 1500 K and upon cooling down into the undercooled liquid state and into the solidified state.

III. RESULTS AND DATA ANALYSIS: FIELD AND TEMPERATURE DEPENDENCE OF MAGNETIC PROPERTIES

A. Paramagnetic concentration range ($x > x_c$)

1. *Magnetic properties for $T \leq 300$ K*

As described above, at sufficiently high P contents, the Ni-P alloys are fully amorphous and, at a given temperature, their magnetization (σ) can be separated into a small ferromagnetic contribution, $\sigma_s(T)$, being saturated for magnetic fields $H \geq H_s$ (according to our experience H_s varied typically from 2 to 4 kOe) and into a linear term characterized by the temperature-dependent initial susceptibility $\chi_0(T)$. In this manner, for magnetic fields $H \geq H_s$ the magnetization can be described as

$$\sigma(H,T) = \sigma_s(T) + \chi_0(T)H \ . \tag{1}$$

The susceptibility $\chi_0(T)$ can be written for the whole temperature range as

$$\chi_0(T) = \chi_{nm} + C_{CW}/(T+\Theta) \ , \tag{2}$$

where χ_{nm} is a temperature-independent susceptibility and the second term is a Curie-Weiss-type susceptibility with the constant C_{CW} and characteristic temperature Θ.

In agreement with the conclusions of Amamou and Durand,[10] we also attribute the FM magnetization component to crystalline Ni or Ni(P) precipitates. The CW term can be ascribed to the presence of giant-moment paramagnetic clusters consisting of Ni-rich amorphous regions embedded in the amorphous matrix. The temperature-independent susceptibility χ_{nm} can be associated with the contribution of nonmagnetic atoms of the amorphous phase and, after correcting for the ion-core diamagnetic susceptibility (χ_{dia}^{core}), it is mainly due to the Pauli paramagnetism of electrons in conduction bands. The conduction electron susceptibility χ_{cond} is obtained as

$$\chi_{cond} = \chi_{nm} - \chi_{dia}^{core} \ . \tag{3}$$

Melt-quenched Ni-P alloys. Of this series, the $Ni_{100-x}P_x$ alloys with $x = 17.3$, 19.8, 20.2, 20.9, and 21.0 were investigated at low temperatures. The magnetization isotherms and the temperature dependence of $\chi_0(T)$ are shown for $x = 21.0$ in Fig. 1, demonstrating that the

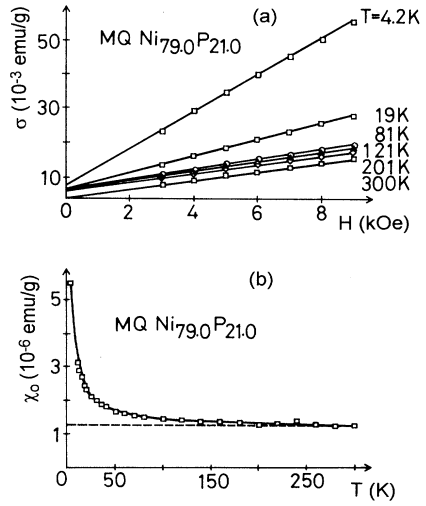

FIG. 1. Low-temperature magnetization isotherms (a) and temperature dependence of the matrix susceptibility χ_0 (b) for a MQ $Ni_{100-x}P_x$ amorphous alloy with $x = 21.0$. The solid lines through the data points represent the fits to Eq. (1) in (a) and to Eq. (2) in (b). The dashed line in (b) corresponds to the temperature-independent susceptibility χ_{nm} in Eq. (2).

experimental data can be well described for $H \geq 4$ kOe by Eqs. (1) and (2). It can also be seen that $\sigma_s(T)$ is very small (at $T=300$ K, it corresponds to about 80 wt ppm crystalline Ni) and shows only a slight variation over the temperature range investigated, indicating a Curie point well above 300 K. Qualitatively, the same behavior was observed for the other alloys as well: linear magnetization isotherms for at least 4 kOe $\leq H \leq 9$ kOe and good CW-type temperature dependence of $\chi_0(T)$ with the assumption of a temperature-independent χ_{nm}. The magnitude of $\sigma_s(4.2\ \text{K})$ remained below about 10×10^{-3} emu/g, C_{CW} varied typically from 5 to 22 in 10^{-6} K emu/g units, and Θ ranged from 0 to $+2.5$ K. The susceptibility χ_{nm} was below 2×10^{-6} emu/g for each composition and decreased with increasing P content. The qualitative features obtained here are in good agreement with the results of Hines *et al.*[22] on MQ amorphous alloys with nominal compositions $18 \leq x \leq 22$.

Electrodeposited alloys. The low-temperature magnetization study of ED alloys with $x=18.5$, 18.7, 19.3, 21.4, 22.3, 23.0, and 23.2 showed that for $x \geq 18.7$ the magnetization isotherms were linear for at least $H \geq 4$ kOe in the temperature range investigated and, similarly to the MQ alloys, they could be well fitted by Eqs. (1) and (2). Also, the susceptibility χ_{nm} decreased systematically with increasing P content. For all of the ED alloys with $x \geq 18.7$, the saturation magnetization of the FM component was found to be again small and weakly temperature dependent [the value of $\sigma_s(4.2\ \text{K})$ remained below about 10×10^{-3} emu/g except for $x=18.7$ where it was about 30×10^{-3} emu/g]. The values of C_{CW} and Θ reduced to practically zero in our ED alloys with the highest P contents but both parameters started to increase more rapidly below $x=19$. This fact and the large increase of $\sigma_s(T)$ at low temperatures already indicate that a different magnetic behavior sets in below about $x=19$ in the ED alloys. This is further substantiated by the data for the ED alloy with $x=18.5$: although the magnetization isotherms could still be reasonably well fitted to Eqs. (1) and (2), the magnitude and temperature dependence of $\sigma_s(T)$ and the value of C_{CW} were much larger than for $x=18.7$. The magnetization isotherms of these two alloys shown in Fig. 2 demonstrate the rapid increase of the magnetization of ED Ni-P alloys below 19 at. % P. Due to the dominance of the contribution of the magnetic inhomogeneities to the total magnetization, no reliable value of χ_{nm} could be deduced for $x=18.5$. This alloy represents already an intermediate state between the paramagnetic ED alloys ($x \gtrsim 19$) and those to be described in Sec. III B for $x \lesssim 17$.

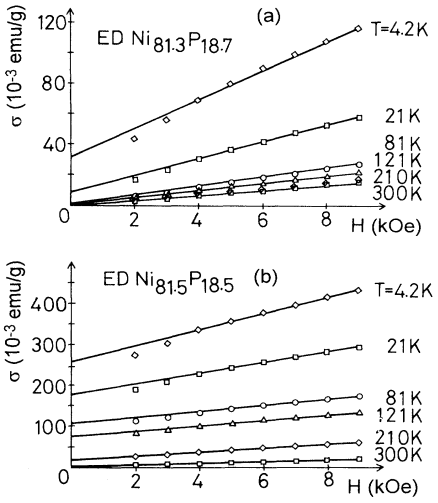

FIG. 2. Low-temperature magnetization isotherms of ED $Ni_{100-x}P_x$ amorphous alloys with $x=18.7$ (a) and $x=18.5$ (b). The straight lines correspond to the fits according to Eq. (1).

2. *Magnetic properties for $T \geq 300$ K*

The high-temperature magnetic susceptibility studies were performed for MQ alloys with $x=16.3$, 16.5, 17.3, 18.4, 19.1, 19.8, 20.5, 20.6, 20.9, and 21.0.

As-quenched amorphous state (300 K $\leq T \leq$ 550 K). Honda-Owen plots were used to evaluate the room-temperature magnetization isotherms and these plots were straight lines for all the MQ Ni-P alloys. The room-temperature susceptibilities derived here agreed well with corresponding data of the low-temperature study and the same holds true also for σ_s (300 K) in most cases. Comparable values of both χ_0 (300 K) and σ_s (300 K) were obtained also for most of the alloys which were not measured below room temperature. Figure 3 shows the results of the high-temperature magnetic susceptibility analysis for a MQ $Ni_{100-x}P_x$ alloy with $x=21.0$ (same sample as in Fig. 1). From the minimum value of χ_H between 300 K and the Ni-precipitation peak, an estimate was made for the temperature-independent susceptibility χ_{nm} by correcting for the contribution of the temperature-dependent $\sigma_s(T)$ to $\chi_H(T)$. Where it was possible, an approximate value or at least an upper limit was estimated for C_{CW} from the $\chi_H(T)$ data for $300 \leq T \leq 550$ K and similar values were obtained as from the low-temperature studies on corresponding compositions. The quantity χ_{nm} derived from measurements above room temperature was in good agreement in most cases with the low-temperature data.

Liquid state (1100 K < T < 1500 K). The inset in Fig. 3 demonstrates that above the melting point indicated by the susceptibility drop (above about 1100 K), χ_H varies nicely linearly with temperature as observed for the previously studied Ni-B-P system as well.[20] The same behavior was obtained for the liquid state of all the other MQ alloys. Since the melting point of these Ni-P alloys is almost twice as high as the Curie point of crystalline Ni (631 K), we may consider that the measured susceptibility, χ_H, in the liquid state does not contain contributions from ferromagnetic precipitates and Curie-Weiss-type clusters. Therefore the liquid-state susceptibility $\chi_l \equiv \chi_H$ corresponds to the quantity χ_{nm} of the amorphous state. The slope $d\chi_l/dT$ of the susceptibility in the liquid state was found to be positive with values ranging from about $+0.020$ to about $+0.038$ in units of 10^{-6} emu/(mol K).

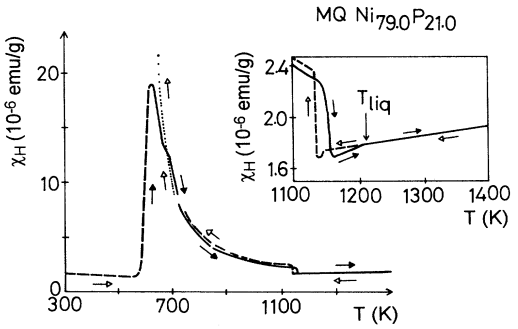

FIG. 3. Magnetic susceptibility χ_H measured at $H=17$ kOe for the MQ $Ni_{100-x}P_x$ amorphous alloy with $x=21.0$ (same alloy as in Fig. 1) as a function of temperature from $T=300$ to 1500 K. The large peak corresponds to the precipitation of Ni during crystallization and the inset shows the susceptibility in the liquid state on an enlarged scale.

A comparison of the χ_{nm} values of the amorphous and liquid states as a function of composition will be presented in Sec. IV B.

B. Magnetic properties of ED Ni-P alloys for $x < x_c$

1. Magnetization isotherms

Here we shall describe the results of low-temperature magnetic studies for ED alloys with $x \lesssim 17$. These investigations were performed on ED samples with $x=11.5$, 12.2, 13.2, 13.6, 13.9, 15.5, 17.0, and 17.2. As already indicated in Sec. III A 1, there is an increase of the magnetization and a change in the magnetic behavior of ED Ni-P alloys when decreasing the P content down to below 19 at. %. The magnetization isotherms at and somewhat below room temperature remain linear for $H \geq 4$ kOe, with small values of $\sigma_s(T)$, for all compositions down to $x=11.5$. On the other hand, for intermediate and low

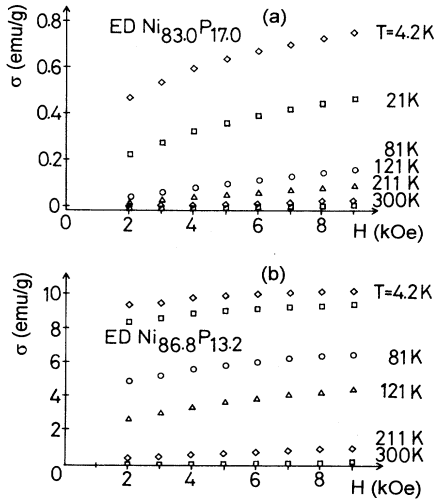

FIG. 4. Low-temperature magnetization isotherms of the ED $Ni_{100-x}P_x$ alloys with $x=17.0$ (a) and $x=13.2$ (b).

temperatures, a characteristic change of the magnetization isotherms can be observed with decreasing x: at higher P contents the low-temperature isotherms become first nonlinear practically for the whole range of magnetic fields and with strongly increased apparent $\sigma_s(T)$ saturation values [Fig. 4(a), $x=17.0$]. At the lowest P contents, the isotherms around the liquid-He temperature become more linear with large apparent saturation magnetization values whereas the isotherms at intermediate temperatures tend to show even less linearity, as for high P contents [Fig. 4(b), $x=13.2$]. The observed rapid increase of the magnetization for $x < x_c$ is in good qualitative agreement with the results of previous studies.[2,4–6,8,23]

2. Data analysis: The Stoner-Edwards-Wohlfarth model of very weak itinerant ferromagnetism

The magnetization isotherms of ED Ni-P alloys for concentrations $x < x_c$ will first be analyzed on the basis of the theory[24] developed, within the framework of the itinerant electron model of Stoner, for describing the magnetic behavior of homogeneous very weak itinerent ferromagnets.

It is customary to introduce the relative magnetization

$$\zeta=\zeta(H,T)=\sigma(H,T)/(nN_g\mu_B)\ . \tag{4}$$

Here, $\sigma(H,T)$ is the magnetization arising from single-particle excitations, n the number of particles per atom, N_g the number of atoms per gram, and μ_B the Bohr magneton. The value of ζ at 0 K, $\zeta_0=\zeta(0,0)$, can be used to distinguish between different kinds of ferromagnets. If the Fermi level lies above the top of the spin-up band and intersects the spin-down band only (e.g., for fcc Ni metal), the magnetization is determined by the number of particles per atom (holes in the minority-spin band) and, therefore, we have $\zeta_0=1$: this case is called strong itinerant ferromagnetism (SIF). If the Fermi level intersects both the spin-up and spin-down subbands (e.g., for bcc Fe metal), the magnetization equals the difference between the holes in the two subbands which leads to $\zeta_0<1$: this is the case of weak itinerant ferromagnetism.

Very weak itinerant ferromagnetism (VWIF) is obtained when $\zeta_0 \ll 1$, which corresponds to the case when the Fermi level intersects both spin subbands but the exchange splitting of the subbands is very small. It has been shown for VWIF's (Ref. 24) that their magnetization can be described by the expression

$$[\sigma(H,T)]^2=[\sigma(0,0)]^2[\,1-(T/T_c)^2 + 2\chi(0,0)H/\sigma(H,T)] \tag{5}$$

in the temperature range $T \ll T_F$ where T_F is the effective degeneracy temperature which depends on the electronic density of states $N(E_F)$ at the Fermi level and on its derivatives at E_F, T_c is the Curie temperature and $\chi(0,0)=[\partial\sigma(H,T)/\partial H]_{H=0,T=0}$ is the differential susceptibility at $T=0$ K and $H=0$ (it also holds that $T_c \ll T_F$). Edwards and Wohlfarth[24] have calculated the magnetization versus field isotherms for $0 \leq T \leq 2T_c$ in

the form of $s=\sigma(H,T)/\sigma(0,0)$ vs $h=\chi(0,0)H/\sigma(0,0)$ plots up to $h=12$. According to these curves, the magnetization isotherms are strongly nonlinear and do not saturate even at very high magnetic fields. Such a behavior could indeed be successfully demonstrated for the typical VWIF $ZrZn_2$.[25]

Equation (5) also implies that plots of σ^2 vs H/σ at various temperatures for $T \ll T_F$ should yield a series of parallel straight lines and for their intersections on the σ^2 axis (i.e., $H=0$), we have the relation

$$[\sigma(0,T)]^2=[\sigma(0,0)]^2[1-(T/T_c^2)] . \quad (6)$$

It follows from Eq. (6) that the temperature for which the straight line on the σ^2 vs H/σ plot passes through the origin yields the Curie point T_c.

Expression (5) derived in the Stoner-Edwards-Wohlfarth (SEW) model[24] was already previously obtained,[26] based on the Landau theory of phase transitions, for temperatures around T_c and the σ^2 vs H/σ plots (so-called Arrott plots) have often been successfully applied for analyzing the behavior of materials with nonlinear magnetization curves. For the case of VWIF's where the magnetization is small and assumed to be spatially homogeneous, the Landau theory applies for the wider temperature range $0 \le T < 2T_c$ and Mathon[27] has obtained the expression

$$A(T)+B(T)\sigma^2(H,T)=H/\sigma(H,T) . \quad (7)$$

It follows from Eq. (7) that $1/B(T)$ is the slope of the straight lines in the Arrott plots (σ^2 vs H/σ) whereas the intercept of these lines with the H/σ axis [i.e., $\sigma^2(0,T)=0$] equals the parameter $A(T)$ which is related to the zero field differential susceptibility, $\chi(0,T)=[\partial\sigma(H,T)/\partial H]_{H=0}$, via the formula[28] $A(T)=-[2\chi(0,T)]^{-1}$.

For the present ED Ni-P alloys with $x<x_c$, the σ^2 vs H/σ plots yielded straight lines for each composition for not too low magnetic fields up to temperatures somewhat above T_c. However, characteristic deviations from linearity occurred at low magnetic fields which can be ascribed to a certain degree of spatial heterogeneity of the magnetization,[24,27,29,30] arising either from demagnetizing effects or from spatial fluctuations of the alloy composition. Typical Arrott plots for temperatures in the vicinity of T_c are shown in Fig. 5 for $x=11.5$ and 15.5.

First, we have determined the intersections $\sigma^2(0,T)$ obtained by extrapolating the straight line portions of the Arrott plots to the σ^2 axis (i.e., to $H=0$). The dependence of $\sigma^2(0,T)$ on T^2 is shown in Fig. 6 for most of the ED alloys with $x \lesssim 17$. According to the SEW model [see Eq. (6)], a straight line is expected to result in this way, which is obviously not the case for any of the alloys investigated here. It should be noted that the same kind of curvature can be observed also for the ED Ni-P amorphous alloys studied by Berrada *et al.*[5,31] as well as by Pan and Turnbull.[4] This clearly indicates that the observed curvature in Fig. 6 is not a specific feature of our alloys but seems to be common to the ED Ni-P system even if the magnetic measurements are extended up to $H=150$ kOe as in the study of Berrada *et al.*[5,31]

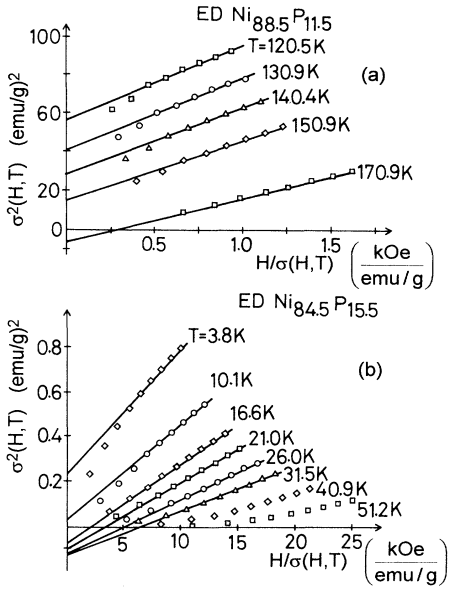

FIG. 5. Arrott plots (σ^2 vs H/σ) for the ED Ni alloys with $x=11.5$ (a) and $x=15.5$ (b).

In spite of the deviation from the linearity, the data points on the $\sigma^2(0,T)$ vs T^2 plots (Fig. 6) can be well averaged by a continuous curve joining smoothly the data below and above T_c. We have used these plots to determine the Curie temperature as the points where these smooth curves crossed the T^2 axis. For the determina-

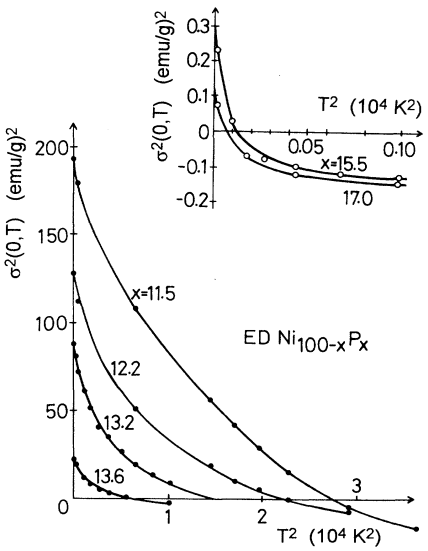

FIG. 6. Plots of $\sigma^2(0,T)$ obtained by extrapolating the linear portions of the Arrott plot to the σ^2 axis (i.e., to $H=0$) as a function of T^2 for our ED $Ni_{100-x}P_x$ alloys with $11.5 \le x \le 13.6$. The inset shows the same plots for $x=15.5$ and 17.0. The plots for $x=13.9$ and 17.2 actually coincide with those of the neighboring compositions and, therefore, they are omitted for clarity. The lines are drawn as a guide for the eye only.

tion of the saturation magnetization at $T=0$ K, $\sigma(0,0)$, we used the data points at the lowest temperature, i.e., $\sigma(H=0, T\cong 4.2\ \text{K})\equiv\sigma(0,0)$ was assumed. This gives definitely somewhat underestimated values of $\sigma(0,0)$ but this deviation amounts up to a few percent only at most (and the relative error is probably the same for each alloy) as shown by Fig. 7 where $\sigma(0,T)$ is plotted against T for our ED alloys.

It should be noted that plots of $\sigma^2(0,T)$ vs T yielded straight lines for the alloys with $11.5\leq x\leq 13.9$ in the low-temperature range up to about $0.5T_c$; upon further approaching T_c, mostly an upward curvature occurred.

We have evaluated also the slopes and the intercepts with the H/σ axis of the straight lines of the Arrott plots. Similarly to the case of $\sigma^2(0,T)$, the temperature dependence of $A(T)$ also did not follow the T^2 law. However, from the low-temperature data we extrapolated $A(T)$ for $T\rightarrow 0$ to get $A(0)$ from which $\chi(0,0)$ could be obtained. As to the slope, $1/B(T)$, of the Arrott plot straight lines, it was found to be approximately temperature independent for the lowest temperatures but started to decrease very strongly with increasing temperature well below T_c. By taking the value $1/B(0)$, we determined $\sigma^2(0,0)$ via the formula[28] $1/B(T)=2\sigma^2(0,T)\chi(0,T)$ by using the value of $\chi(0,0)$ as obtained above from $A(0)$, and these $\sigma^2(0,0)$ values were within a few percent of those derived from the plots in Fig. 6.

We have, in this manner, a consistency in the data evaluated from the Arrott plots and we should now look for the possible origins of deviation from the quadratic temperature dependence predicted by the SEW model [Eq. (6)]. These deviations may originate from either of or both of two sources.

(a) The experimental values of $\sigma(0,T)$ as determined with the help of the straight lines of the Arrot plots contain also contributions from a magnetic component the behavior of which cannot be described by the SEW model. A way of separating out such a contribution from the VWIF term has been discussed by Acker and Huguenin.[32] In the case of the ED Ni-P alloys, these magnetic inhomogeneities behave as superparamagnetic particles

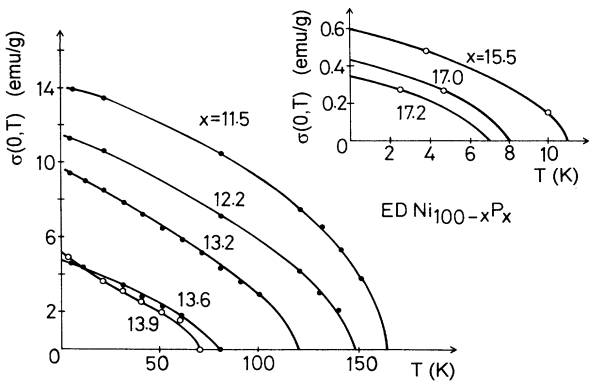

FIG. 7. The same data as in Fig. 6 displayed as $\sigma(0,T)$ vs T plots for our ED Ni-P alloys. The lines are drawn as a guide for the eye only, by taking into account the T_c values as determined in Fig. 6.

as will be described in Secs. III B 3 a and III B 3 b.

(b) Some of the basic assumptions of the SEW model are not valid for the VWIF matrix of the sample.

(i) The SEW model takes into account individual (single-particle) excitations[24] only whereas subsequent theoretical studies[33,34] have demonstrated that collective spin fluctuations may, under certain circumstances, also play a significant role and experimental evidence for this behavior has, indeed, been found for the amorphous Y-Ni system.[35] One main effect of collective spin fluctuations is that, in contrast to Eq. (6), $\sigma^2(0,T)$ does not vary with temperature as T^2. An analysis of the temperature dependence of $\sigma^2(0,T)$ for the ED Ni-P alloys in terms of this model will be given in Sec. III B 3 c.

(ii) It has been shown[27] that the SEW model describes the magnetic behavior of itinerant ferromagnets only if the magnetization is spatially homogeneous. Apart from the influence of demagnetizing effects at low applied magnetic fields ($H\leq H_s$), another cause for the spatial heterogeneities of the magnetization may be the fluctuation of the chemical composition, resulting in a local variation of the spontaneous magnetization [too strong compositional fluctuations may lead to the situation described in item (a) above]. A theoretical study of the effect of compositional fluctuations on the Arrott plots has been performed by Wohlfarth and co-workers.[30,36,37] A comparison of the curvature of Arrott plots for our ED Ni-P alloys observed in the present study and in previous works[4,5,31] with those calculated theoretically[30,36] would suggest that the compositional fluctuations in the VWIF phase of the ED Ni-P alloys may not, indeed, be very large.

3. *Data analysis: beyond the homogeneous SEW model*

a. Appearance of superparamagnetic particles for $x\lesssim 17$. As indicated by the data on ED alloys with $x>x_c$ (Sec. III A 1), the Curie-Weiss-type contribution to the observed magnetization starts to increase rapidly as the P content decreases to below 19 at. %. This can be ascribed to the increase of either the size or the concentration (or both) of the giant-moment paramagnetic clusters. At sufficiently low P contents, the size of the giant-moment clusters can increase to the extent that they become ferromagnetic at low temperatures but the coupling between spins within the clusters is still not strong enough to retain a spontaneous magnetization at those temperatures where bulk samples of the same chemical composition would exhibit ordinary ferromagnetism. In such a case we have to deal with superparamagnetic (SPM) particles.

Figure 8 demonstrates that for the samples with $x=17.2$, 17.0, and 15.5, the magnetic behavior is dominated by the contribution of SPM particles: above the ordering temperature, the magnetization (σ) data when plotted against H/T fall on a universal curve which can be approximately described by the formula for superparamagnetic particles:[38]

$$\sigma(H,T)=\sigma_s\left[\coth\left(\frac{\bar{\mu}H}{kT}\right)-\frac{kT}{\bar{\mu}H}\right], \tag{8}$$

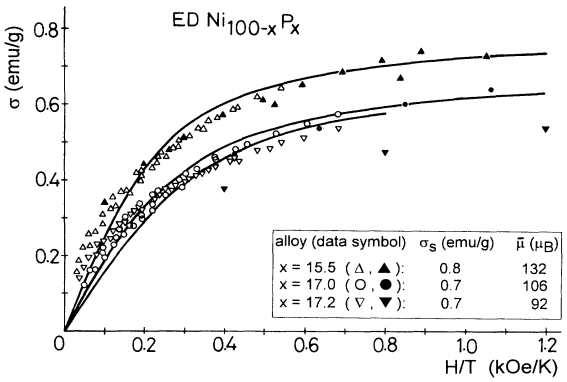

FIG. 8. Measured magnetization σ against H/T for the ED $Ni_{100-x}P_x$ alloys with $x=15.5$ ($\triangle$,$\blacktriangle$), $x=17.0$, ($\circ$,$\bullet$), and $x=17.2$ (∇,$\blacktriangledown$). The magnetic field range was 1 kOe $\leq H \leq 9$ kOe. The light and solid symbols correspond to data obtained at temperatures $T_c < T < 40$ K and $T < T_c$, respectively. The solid lines correspond to curves according to Eq. (8) with the saturation magnetization σ_s of the assembly of SPM particles and average magnetic moment $\bar{\mu}$ of a SPM particle as given in the inset.

where $\sigma_s = N\bar{\mu}$ is the saturation magnetization per gram of the assembly of SPM particles, $\bar{\mu}$ is the average magnetic moment of a particle, and N is the number of SPM particles per gram. Obviously, the scatter of the data and the quality of the fit would have been improved if we had accounted for the temperature dependence of the saturation magnetization. The systematic deviation between experimental data and fitted curves at low values of H/T can originate from the presence of a small amount of a ferromagnetic contribution. At temperatures below T_c as derived from the Arrott plots, significant deviations from SPM behavior occur, indicating that this T_c value corresponds approximately to the temperature below which the SPM particles already exhibit the usual FM behavior. A further refinement could have certainly been made by introducing a distribution[39,40] of the average particle moment $\bar{\mu}$ and accounting also for a paramagnetic matrix contribution.

In spite of these apparent weaknesses of the fit to the experimental data, we have evaluated the fitted parameters according to Eq. (8) and the values of σ_s and $\bar{\mu}$ are given in the inset in Fig. 8. For the alloy with $x=15.5$ for which $N=6.6\times10^{17}$/g, we can thus derive, from $\sigma_s = N\bar{\mu}$, that an average particle consists of about 220 Ni atoms. By assuming that each Ni atom in the SPM particles possesses a magnetic moment of $0.6\mu_B$ as in bulk fcc Ni, we obtain that only about 1.6% of the Ni atoms is situated in SPM particles. This means that the majority of the Ni atoms in the sample is still in a paramagnetic matrix the magnetic behavior of which is completely masked by the SPM particles. Although the values of σ_s and $\bar{\mu}$ are somewhat smaller for $x=17.0$ and 17.2, these alloys show qualitatively the same behavior.

Below $x=15.5$, the magnetic behavior changes again. For $x=13.9$, the σ vs H/T curves do not fall on each other for temperatures around T_c even if we correct for the temperature dependence of σ_s. This change can be attributed to the fact that the matrix for these concentrations already exhibits ferromagnetism upon which the SPM is still superimposed as discussed in the next section.

b. Coexistence of VWIF and SPM. In a study of the PM-FM transition of Ni-based alloys, Acker and Huguenin[32] analyzed in detail the magnetic behavior of a VWIF matrix in which SPM particles are embedded. An important feature of this analysis is that, when deriving the expressions for the Arrott plots, the external magnetic field should be increased by an amount $\lambda\sigma_s$ which can be considered as a molecular field characterized by the constant λ due to the presence of SPM particles with large magnetic moments in the VWIF matrix. They have also pointed out that, due to this interaction between the matrix and the particles, the presence of the magnetic inhomogeneities is not necessarily to alter the straightness and parallelism of the Arrott plots. They have shown, on the other hand, that an analysis of the temperature dependence of the derivative $d\sigma(H,T)/dT$ of the total measured magnetization in a constant high field H leads to characteristics which allow us to easily identify and to separate the influence of SPM particles in a VWIF matrix.

We now apply this representation for our ED $Ni_{100-x}P_x$ alloys with $x \leq 15.5$. The temperature dependence of $d\sigma(H,T)/dT$ obtained in our highest magnetic field of $H=9$ kOe is shown in Fig. 9 for the ED $Ni_{88.5}P_{11.5}$ alloy. The experimental data follow a curve which has a peak around the T_c value derived from the

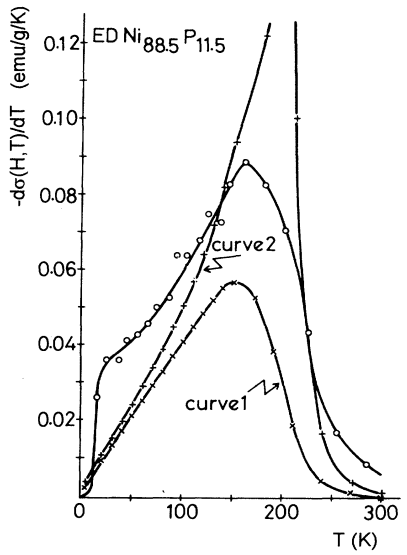

FIG. 9. Temperature derivative of the measured magnetization $d\sigma(H,T)/dT$ for the ED $Ni_{88.5}P_{11.5}$ alloy at $H=9$ kOe ($\circ$: experimental data; the solid line through the data serves as a guide for the eye only). The curves labeled 1 and 2 refer to $d\sigma(H,T)/dT$ vs T curves according to Eq. (9) of the SEW model for a homogeneous VWIF matrix having $T_c=164$ K with $\chi(0,0)^{-1}=0.0066\times10^6$ and 0.0132×10^6 g/emu, respectively.

Arrott plot and also has a shoulder around 20 K. A comparison of Fig. 9 with the experimental data and with the simulated curves of Acker and Huguenin[32] for Ni-Pt and Ni-V alloys around the PM-FM transition clearly reveals that also for our ED $Ni_{88.5}P_{11.5}$ alloy we have to deal with the coexistence of VWIF and SPM.

For a homogeneous VWIF matrix, we have from Eq. (5) that

$$\frac{d\sigma(H,T)}{dT}=\frac{-T\sigma(H,T)}{[1-T^2/T_c^2+3\chi(0,0)H/\sigma(H,T)]T_c^2} . \quad (9)$$

If we apply this expression for the $Ni_{88.5}P_{11.5}$ alloy with values of $\chi(0,0)$ and T_c as derived from the Arrot plots, we get the temperature dependence of $d\sigma(H,T)/dT$ in the homogeneous SEW model. This temperature derivative is also shown in Fig. 9 for two values of $\chi(0,0)$. The lower curve was obtained with the $\chi(0,0)$ value from the Arrott plot analysis. However, the $\chi(0,0)$ values obtained in this manner probably have a large error and they show a significant scatter as a function of the P content (see later in Sec. IV C). If we take a smoothed average for the concentration dependence of $\chi(0,0)$, we get a value half that derived from experiment and in Fig. 9 the upper calculated curve results. Nevertheless, the true value of $\chi(0,0)$ probably lies in between and whereas the experimental peak around T_c is reproduced by both calculated curves, the low-temperature shoulder does not appear. As the simulation of Acker and Huguenin[32] has revealed, this shoulder can be attributed to the presence of SPM particles embedded in the homogeneous VWIF matrix with which they interact magnetically.

Figure 10 shows the experimental $d\sigma(H,T)/dT$ data as a function of temperature for the alloys with $x \leq 15.5$. With increasing P content x, the peak shifts towards lower temperatures corresponding to the decrease of T_c (see Fig. 7). The low-temperature shoulder due to SPM particles is clearly visible for $x=11.5$, 12.2, and 13.2 and is around 20 K for each alloy. For $x=13.9$ (and also for $x=13.6$ not shown in Fig. 10), only a faint hump indicates the position of T_c and the $d\sigma(H,T)/dT$ curve is dominated by the contribution of the SPM particles around 20 K. For $x=15.5$ which is also included in Fig. 10, T_c already completely coincides with the low-temperature peak due to SPM particles.

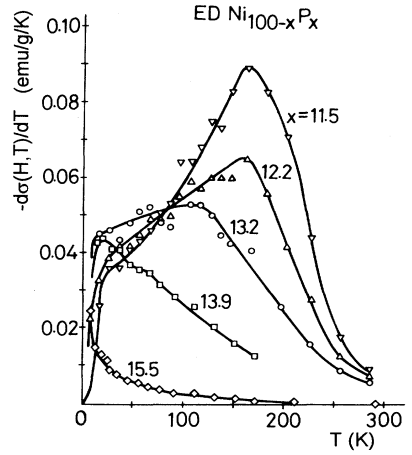

FIG. 10. Experimental $d\sigma(H,T)/dT$ vs T data at $H=9$ kOe for ED $Ni_{100-x}P_x$ alloys with $x=11.5$ (▽), 12.2 (△), 13.2 (○), 13.9 (□), and 15.5 (◇). The solid lines serve as a guide for the eye only.

One may conclude from the above analysis that our ED Ni-P alloys with $x \lesssim 15$ exhibit a VWIF matrix in which SPM particles are embedded. The entity of the SPM particles possesses a saturation magnetic moment σ_s of the order of about 1 emu/g at low temperatures. This means that in this composition range, the saturation magnetization $\sigma(0,T)$ derived from the Arrott plots is probably higher by this amount than the saturation magnetization contribution of the VWIF matrix. It follows from this that the strong upward curvature of the experimental $\sigma^2(0,T)$ vs T^2 plots (Fig. 6) may be partly attributed to the effect of SPM particles and, therefore, the $\sigma(0,0)$ values of the VWIF matrix are probably somewhat overestimated and this fact may partly compensate for the underestimates (Sec. III B 2) due to the assumption $\sigma(0,0)\equiv\sigma(H=0,T\cong 4.2\text{ K})$. It also follows from the analysis of Acker and Huguenin[32] that if SPM particles are present in a VWIF matrix then an Arrott plot evaluation of the experimental data always yields higher values of T_c than the true value of the VWIF matrix without the presence of SPM particles. It appears from their data for some Ni-based alloys that the apparent T_c can be higher by as much as about 100 K than the true Curie temperature and for alloys which could be shown to have a Pauli paramagnetic matrix after removing the contribution of SPM particles, T_c values as high as 40 K were obtained in some cases from the Arrott plots.

c. Influence of collective spin fluctuations. The temperature dependence of the spontaneous magnetization in the SEW model, involving single-particle excitations only and applying the recently developed spin-fluctuation theory can be conveniently described by writing[41,42]

$$\sigma^2(0,T)\propto(T_c^{\eta}-T^{\eta}) , \quad (10)$$

where $\eta_{SEW}=2$, $\eta_{MD}=1$, and $\eta_{MK}=\frac{4}{3}$ and the subscripts MD and MK refer to the results in the models of Murata and Doniach[33] and Moriya and Kawabata,[34] respectively.

For the amorphous Ni-Y system prepared by sputtering, Lienard and Rebouillat[35] obtained that η decreased continuously from 2 for 7 at. % Y to 1 for 16.7 at. % Y (the latter is practically the critical concentration for the disappearance of ferromagnetism). This result indicates that the collective spin fluctuations increase when the magnetization decreases, i.e., the critical concentration of the FM-PM transition is approached from the FM concentration range.

It can be seen in Fig. 11 that for our ED Ni-P alloys around $x=11.5$, Eq. (10) describes the temperature dependence of the spontaneous magnetization with $\eta=1.185$ whereas for $x=12.2$, $\eta=1$ is obtained although the fit is significantly less good. However, for $x=13.9$ the data cannot be described by Eq. (10). These data imply that not too close to the FM-PM transition the collective spin fluctuation theory can give a good

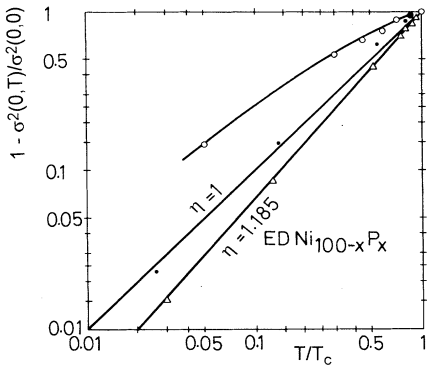

FIG. 11. Temperature variation of the magnetization $\sigma(0,T)$ on a reduced scale for the ED $Ni_{100-x}P_x$ alloys with $x=11.5$ (△), 12.2 (●), and 13.9 (○). The straight lines drawn through the data points for $x=11.5$ and 12.2 indicate a fit according to Eq. (10) with η as given on the lines; the data for $x=13.9$ do not follow a straight line and, therefore, could not be fitted to Eq. (10).

description of the temperature dependence of $\sigma(0,T)$ of the FM phase whereas in the immediate vicinity of the critical concentration of the disappearance of ferromagnetism, which is about 14 to 14.5 at. % P for our samples (see Sec. IV), the interplay between the contributions due to the SPM particles and the VWIF matrix (see Sec. III B 3 b) masks this behavior. Furthermore, the linearity of the $\sigma^2(0,T)$ vs T plots up to about $0.5T_c$ indicates that for low temperatures, again, the collective spin fluctuations give the dominant contribution to the temperature variation of the spontaneous magnetization and this may be mixed at higher temperatures with the SPM contribution.

We have performed the analysis based on Eq. (10) also for the magnetization data reported by Berrada *et al.*[5,31] and Pan and Turnbull[4] on ED Ni-P alloys. It was obtained again that for alloys not too close to the FM-PM transition, Eq. (10) describes well the data with $\eta=1$, whereas in the vicinity of the FM-PM transition the same kind of deviation from Eq. (10) occurs as shown for our alloys in Fig. 9.

Recently, Tolkachev and Yurasov[43] have achieved a further refinement of the spin fluctuation theory. They derived an expression according to which, over most of the temperature range below T_c, the decrease of $\sigma^2(0,T)$ is described by the sum of a T^2 and a $T^{4/3}$ term. This mixed temperature dependence law was found to explain properly the behavior of $ZrZn_2$ and corresponds to the same type of upward curvature below T_c as obtained for our ED Ni-P alloys (Fig. 6).

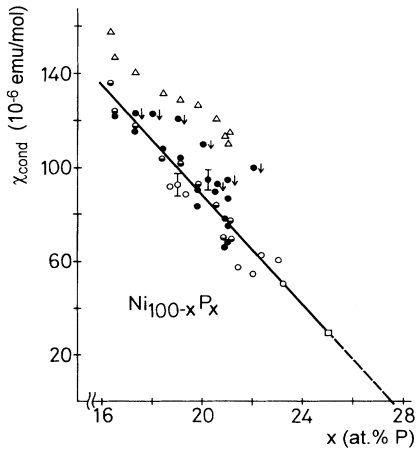

FIG. 12. Conduction electron susceptibility χ_{cond} vs P content x in paramagnetic Ni-P alloys (○: ED, amorphous; ●: MQ, amorphous; ●↓: MQ, amorphous, upper limit only; △: melt, $T=1400$ K; ◒: melt, extrapolated to $T=300$ K; □: crystalline Ni_3P). The MQ data for $x=18$, 19, 20, 21, and 22 labeled by ●↓ are from Ref. 22; for crystalline Ni_3P, the value given is from Ref. 44 where the matrix susceptibility was properly determined by separating the contribution of magnetic inhomogeneities whereas previous studies of Ni_3P (Refs. 3 and 45) yielded much larger values probably due to the lack of such a separation.

IV. DISCUSSION: DEPENDENCE OF MAGNETIC PROPERTIES ON COMPOSITION AND PREPARATION TECHNIQUE

A. Composition dependence of the conduction electron susceptibility in the Pauli paramagnetic phase ($x > 17$)

In Sec. III A, the conduction electron susceptibility χ_{cond} was deduced from the experimental data for ED and MQ $Ni_{100-x}P_x$ amorphous alloys with $x \gtrsim 17$ and for the molten state of MQ alloys. For the amorphous alloys, a temperature dependence of χ_{cond} could not be traced out whereas a linear temperature dependence of χ_{cond} in the liquid state could be established (see Fig. 3) and, in this manner, an extrapolated room-temperature susceptibility could also be determined for the molten state alloys.

Figure 12 summarizes the results of the susceptibility measurements on paramagnetic Ni-P alloys together with the data of Hines *et al.*[22] on MQ samples. It can be established that (i) χ_{cond} has practically the same value for a given P content in both the ED and MQ alloys; (ii) the χ_{cond} values of the melt when extrapolated to room temperature agree well with the data for the amorphous state at the same composition; and (iii) the χ_{cond} values decrease nearly linearly with increasing P content, extrapolate through the data for the crystalline Ni_3P phase, and go to 0 at about 27 at. % P.

Due to the almost completely filled d bands of paramagnetic Ni-P alloys,[46,47] the orbital susceptibility contribution can be assumed very small. Therefore χ_{cond} can be identified with the Pauli paramagnetic susceptibility of the conduction electrons. Since this contribution is determined by the electronic density of states at the Fermi level, $n(E_F)$, the experimental data in Fig. 12 also indicate that $n(E_F)$ decreases significantly with increasing P content. This feature is in good agreement with the general behavior of the composition dependence of

$n(E_F)$ in Ni-metalloid alloys as deduced from low-temperature specific heat data[46] and from theoretical band-structure calculations.[47]

B. Magnetic inhomogeneities at the PM-FM transition and influence of preparation method

The composition dependence of the parameters σ_s(300 K), C_{CW}, and Θ characterizing the magnetic inhomogeneities is shown in Figs. 13, 14, and 15, respectively, for both types of alloys.

According to Fig. 13, σ_s(300 K) remained fairly small for the ED $Ni_{100-x}P_x$ alloys above about 18.5 at. % P and did not show a systematic composition dependence. For the MQ alloys, σ_s(300 K) also remained small in the middle of the composition range studied and showed large values at compositions approaching both ends of the glass-formation range which is centered approximately at the eutectic composition.

The formation of the giant-moment clusters exhibits a somewhat different composition dependence for the two preparation techniques. The Curie-Weiss constant C_{CW} (Fig. 14) is again fairly small for the ED alloys with $x \gtrsim 20$ but it starts to increase very rapidly when the P content goes below about 19 at. %. For the MQ alloys, C_{CW} shows an apparently similar composition dependence as σ_s(300 K) did, but the upturns at the ends of the composition range studied are much smaller and it might probably be more appropriate to say that C_{CW} remains practically constant at fairly low values over the whole concentration range. Figure 15 shows the composition dependence of Θ: it remains practically constant around 1 to 3 K for the MQ alloys and starts to increase rapidly with decreasing P content around $x = 19$ for the ED alloys, similarly to C_{CW}. It should be noted that, for C_{CW} and Θ, there are two alloys which fall out of the general trend described above. However, since the MQ alloy with $x = 20.2$ was prepared from another batch[7] and the ED alloy with $x = 21.4$ was produced under rather extreme, unusual deposition conditions, we may still consider that the data presented in Figs. 14 and 15 do show the systematic behavior described above.

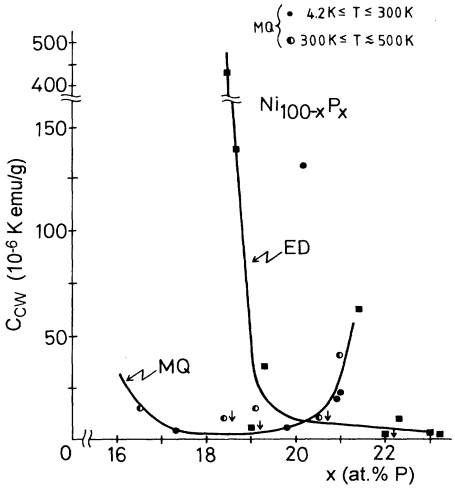

FIG. 14. Composition dependence of the Curie-Weiss constant C_{CW} characterizing the giant-moment paramagnetic clusters in ED and MQ Ni-P alloys. The solid lines serve as a guide for the eye only.

Figures 13–15 demonstrate that there are striking differences in the composition dependence of the occurrence of magnetic inhomogeneities for the ED and MQ preparation process. In the ED technique, alloys are produced in a random, atom-by-atom deposition process. If the P content is sufficiently high and strongly magnetic atoms such as Fe or Co are not present, the formation of large-sized ferromagnetic crystalline precipitates consisting of several thousands of Ni atoms at least is highly im-

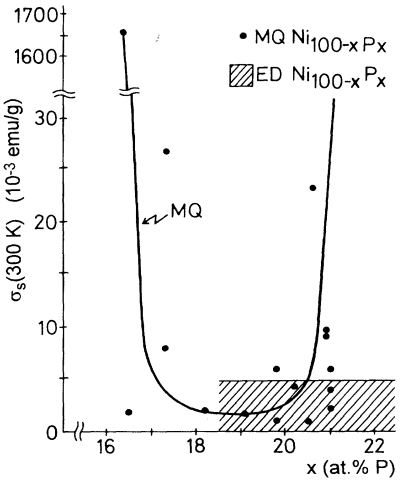

FIG. 13. Composition dependence of the room-temperature saturation magnetization σ_s(300 K) of ferromagnetic precipitates in ED and MQ Ni-P alloys. The solid lines serve as a guide for the eye only.

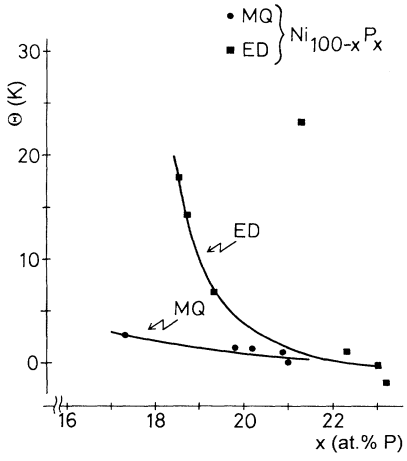

FIG. 15. Composition dependence of the characteristic temperature Θ of the giant-moment paramagnetic clusters in ED and MQ Ni-P alloys. The solid lines serve as a guide for the eye only.

probable since P atoms are also continuously being incorporated into the deposit. The lack of Ni precipitates for $x \gtrsim 18.5$ was, indeed, found (see Fig. 13). On the other hand, the formation of giant-moment PM clusters cannot be excluded in this process at any P content if we consider the generally accepted picture of the structure of transition-metal–metalloid type amorphous alloys.[48] According to this, the basic building block in these glasses is a capped trigonal prismatic arrangement of nine Ni atoms around a central P atom (this structural model excludes first-neighbor P atoms). In a random deposition process, it can frequently happen that a P atom is substituted by a Ni atom and, then, a cluster of at least ten Ni atoms is immediately formed. This process is, of course, gradually enhanced with decreasing P content, partly for probability reasons and also due to the known clustering tendency of Ni atoms when approaching the critical concentration for the onset of ferromagnetism.[9,10] These features can well explain the observed rise of both C_{CW} and Θ as the P content decreases below about 19 at. %.

As for the MQ technique, glass formation in the Ni-P system by this process is restricted to a relatively narrow concentration range (about ± 2 at. % P) around the eutectic composition at about 19 at. % P. In the MQ process, the starting phase is the melt in which the chemical interaction between the different species governs the chemical short-range order (SRO) as in the equilibrium crystalline phases. If the cooling rate during melt quenching is sufficiently high to retain the liquid structure, chemical (i.e., magnetic) inhomogeneities are not expected to occur. Therefore, for Ni-P alloys which could be obtained in an amorphous state by the MQ process, strong giant-moment clusters are also not expected to occur in high amounts as actually observed in Figs. 14 and 15. However, in the case of an insufficient cooling rate, alloy decomposition may take place which should lead, for P contents below 25 at. %, to the appearance of the α phase [crystalline Ni or Ni(P) solid solution precipitates] and to the precipitation of one of the stable crystalline Ni-P phases (probably Ni_3P). The appearance of a larger amount of Ni precipitates also shows up in the magnetic data (Fig. 13) for alloy compositions close to the end of the glass-formation range due to the strong increase of the critical cooling rate. Furthermore, the amount of Ni precipitates is significantly higher on the Ni-rich side where the α-phase formation should be stronger.

It is noted finally that the same assumptions about the types of magnetic inhomogeneities could be used to explain the differences in the crystallization behavior of ED and MQ Ni-P alloys.[21]

C. Composition dependence of magnetic properties in the VWIF phase

It was shown in Sec. III B that the magnetization isotherms of our ED $Ni_{100-x}P_x$ alloys with $x < 15$ could be reasonably well evaluated within the framework of the SEW model of VWIF and the deviations from this theory could also be accounted for. If the SEW model applies, then the quantities $\sigma^2(0,0)$, T_c^2, and $1/\chi(0,0)$ as derived from the Arrott plots should be a linear function of the concentration of the magnetic constituents which are called Mathon plots.[27,28] Therefore, we present in Figs. 16, 17, and 18 these quantities, respectively, as a function of the Ni content c for our ED Ni-P alloys together with data from those previous studies where a similar Arrott plot analysis was performed.

As far as our $\sigma^2(0,0)$ and T_c^2 data are concerned, their variation with Ni content c is nicely linear in the FM concentration range (Figs. 16 and 17) as expected according to the theory of Mathon[27,28] and both plots yield the same value $c_0 \approx 85.7$ at. % Ni for the critical concentration for the onset of FM in Ni-P alloys and the values of these parameters remain negligibly small for $c < c_0$. Although the values of $1/\chi(0,0)$ show a large scatter as a function of c, their variation with concentration for $c > c_0$ also follows, on the average, a Mathon plot and $1/\chi(0,0)$ remains fairly small for $c < c_0$ (Fig. 18).

Available data from the literature for T_c also correspond approximately to a Mathon plot (Fig. 17) although with a larger scatter but with a slope parallel to the Mathon plot of our alloys. However, these previous data yield considerably lower values of c_0 than obtained for our alloys and this large difference in c_0 cannot be attributed to an uncertainty of the chemical composition determination which can be about ± 1 at. %. On the other hand, the data in Fig. 17 can also be interpreted in such a way that Ni-P alloys with a given composition were found to have significantly different T_c values in different studies. This can be perhaps better visualized in Fig. 19 where T_c is shown as a function of the P content. Differences as high as over 100 K were obtained for T_c at a given P content. It was argued in Sec. III B 3 b that the Arrott plot T_c can be apparently higher by as high as this amount if strongly SPM particles are present in the

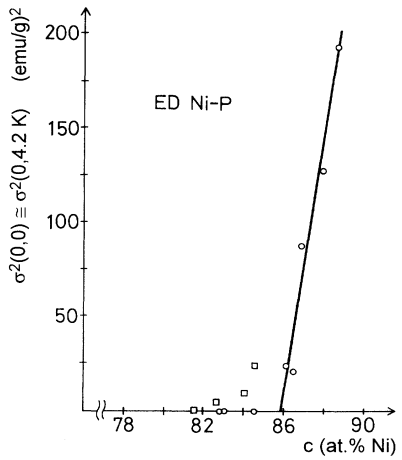

FIG. 16. Composition dependence of the square of the saturation magnetization $\sigma^2(0,0) \cong \sigma^2(0,4.2\ K)$ as derived from the Arrott plots for ED Ni-P alloys around the PM-FM transition (○: this work; □: Refs. 5 and 31). The straight line corresponds to a Mathon plot (Refs. 27 and 28) defining the critical concentration $c_0 \cong 85.7$ at. % Ni for the onset of spontaneous magnetic order in our ED Ni-P alloys.

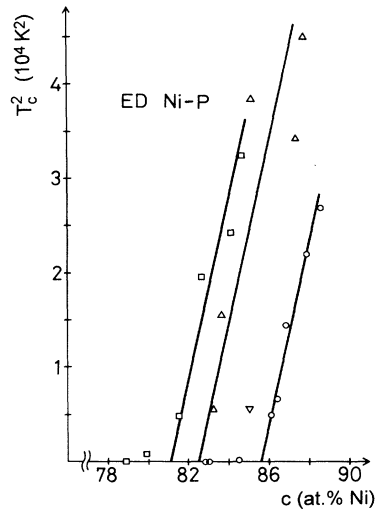

FIG. 17. Composition dependence of the square of the Curie temperature T_c^2 as derived from the Arrott plots for ED Ni-P alloys around the PM-FM transition (○: this work; □: Refs. 5 and 31; △: Ref. 4; ▽: our estimate from the data of Ref. 49). The straight lines correspond to the Mathon plots (Refs. 27 and 28) defining the critical concentration c_0 for the onset of spontaneous magnetic order.

homogeneous VWIF or Pauli paramagnetic matrix. Since in previous studies fairly high T_c values were found (Fig. 19) for P contents where our alloys were definitely Pauli paramagnetic, we may conclude that our Ni-P alloys contained a small amount of magnetic inhomogeneities throughout the whole concentration range studied and the higher T_c values obtained in previous studies can be attributed to a significant amount of SPM particles in those samples. This conclusion is supported by

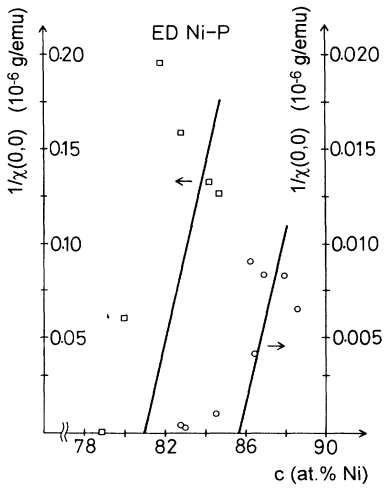

FIG. 18. Composition dependence of the inverse initial susceptibility $1/\chi(0,0)$ as derived from the Arrott plots for ED Ni-P alloys around the PM-FM transition (○: this work; □: Refs. 5 and 31). The straight lines correspond to Mathon plots (Refs. 27 and 28) defining the critical concentration for the onset of spontaneous magnetic order.

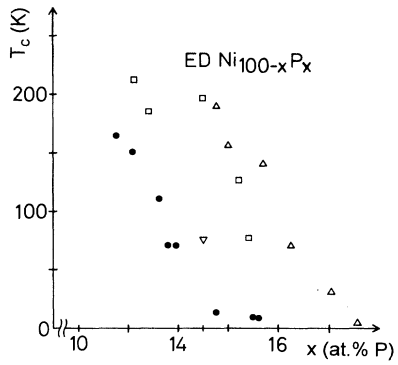

FIG. 19. Composition dependence of the Curie temperature T_c as derived from the Arrott plots for ED Ni-P alloys around the PM-FM transition (●: this work; △: Refs. 5 and 31; □: Ref. 4; ▽: our estimate from the data of Ref. 49).

the saturation magnetization data (Fig. 16) as well since the presence of SPM particles yields an increased value of $\sigma(0,0)$ when derived from the Arrott plot. Since our ED Ni-P alloys also contained some amount of SPM particles, our $\sigma(0,0)$ and T_c values represent to some extent also an upper estimate only and, therefore, the true value of c_0 for the appearance of FM in a homogeneous matrix may be even higher than 85.7 at. % Ni but the deviation must be fairly small.

There are also further data in the literature for the composition dependence of the spontaneous magnetization of Ni-P alloys, especially for lower P contents and Fig. 20 summarizes these results where the saturation magnetization $\sigma_s(0)$ is plotted against the P content. The quantity $\sigma_s(0)$ was obtained here actually by applying Eq. (1) to the magnetic isotherms taken at $T \cong 4.2$ K, i.e., extrapolating the high-field, linear portion of these isotherms to $H=0$. The data of Albert *et al.*[2] for $0<x<10$ fall nicely on the continuation of the straight

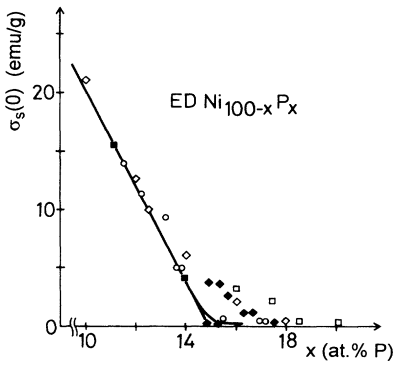

FIG. 20. Composition dependence of the low-temperature saturation magnetization $\sigma_s(0) \equiv \sigma_s(H \to 0, T \cong 4.2$ K) as determined according to Eq. (1) for ED Ni-P alloys around the PM-FM transition (○: this work; □: Refs. 5 and 31; ■: Ref. 2; ◇: Ref. 6; ◆: Ref. 8). The solid line corresponds to a continuation of the average of the $\sigma_s(0)$ vs x data of Ref. 2 for compositions $x<10$ (not shown in the figure) and goes through the $\sigma_s(0)$ value of bulk fcc Ni at $x=0$.

line drawn also as a lower envelope of the data points including our measurements. This plot defines $c = 85$ at. % Ni as the critical concentration for the onset of FM. This is somewhat smaller than that derived from the Arrott plot data for our alloys (85.7 at. % Ni). Since the data for our ED Ni-P alloys can be reasonably well described by the Arrott plot and the Mathon plot, it is believed that the higher value of c is closer to the critical concentration for the onset of FM in the Ni-P system.

V. SUMMARY

A detailed study of the temperature and field dependence of the magnetization of electrodeposited, melt-quenched, and liquid $Ni_{100-x}P_x$ alloys has been described in the present paper. For the ED alloys, the composition range studied ($11 \lesssim x \lesssim 23$) included both the transition between the crystalline and the amorphous phases and the PM-FM transition (the critical concentration being at 85.7 at. % Ni or 14.3 at. % P) whereas all the amorphous MQ alloys investigated here ($17 \lesssim x \lesssim 21$) were found to be paramagnetic. Although magnetization inhomogeneities in the form of ferromagnetic precipitates, giant-moment paramagnetic clusters, or superparamagnetic particles were found to exist throughout the whole concentration range for both ED and MQ alloys, their contribution could be separated out in most cases. It could be established that for $x \gtrsim 17$, the homogeneous matrix of amorphous Ni-P alloys exhibits Pauli paramagnetism characterized by a practically temperature-independent susceptibility whereas for $11 \lesssim x \lesssim 15$, i.e., in the composition range where the transition from the crystalline to the amorphous state occurs, the matrix of Ni-P alloys exhibits VWIF. For $15 \lesssim x \lesssim 17$, the observed magnetization was dominated by the contribution of superparamagnetic particles (it is suggested that the same situation may have occurred in the previously studied chemically reduced Ni-P alloys[50–52] that may well explain their "peculiar magnetic behavior" and probably the same is valid for the ED Ni-P alloys studied by Nelson, Toth, and Judy[53] whose data were not included in our discussion).

In the PM concentration range, the conduction electron susceptibility χ_{cond} decreased approximately linearly with increasing P content and extrapolated through the value of the crystalline Ni_3P compound. Furthermore, χ_{cond} was the same for ED and MQ alloys and, also, the liquid-state susceptibility when extrapolated to 300 K agreed well with χ_{cond} of the amorphous state. These facts indicate that the lack of long-range order does not appreciably influence such macroscopic properties as the Pauli susceptibility and the short-range order of the amorphous phase prepared by either technique probably does not differ significantly from that of the liquid and crystalline states.

On the other hand, the nature and amount of magnetic inhomogeneities in the PM range were found to be different for the ED and MQ technique and their appearance could be explained by the difference in the ways of alloy formation by these two methods. The magnetic inhomogeneities are either crystalline Ni or Ni(P) precipitates or amorphous Ni-rich regions as demonstrated for ED Ni-P alloys with $15 \lesssim x \lesssim 20$ with the help of small-angle x-ray scattering and transmission electron microscopy.[8,12]

It might be appropriate to discuss at this point briefly also the small-angle neutron scattering results of Schild *et al.*[54] on a MQ $Ni_{80}P_{20}$ amorphous alloy. Their conclusion about the existence of regions having the approximate composition $Ni_{75}P_{25}$ seems to be in an apparent contradiction with the finding of Dietz and co-workers[8,12] on ED Ni-P alloys mentioned above. However, as discussed in Sec. IV B, in MQ Ni-P alloys at sufficiently high cooling rates chemical inhomogeneities if at all are expected to occur in the form of Ni and Ni_3P precipitates. Of course, in the hypereutectic alloy $Ni_{80}P_{20}$, the appearance of Ni_3P precipitates (or eventually amorphous regions with compositions close to 25 at. % P) is more preferred than that of the Ni precipitates and, since Ni_3P is paramagnetic with a low susceptibility, they remain unrevealed by the magnetic measurements by which only the Ni precipitates are detected even if their volume fraction is much smaller and, therefore, the latter probably do not give a contribution to the small-angle neutron scattering. Due to the different way of alloy formation, the occurrence of $Ni_{75}P_{25}$-like regions in the matrix of ED Ni-P alloys with $20 \lesssim x \lesssim 25$ is not expected but a small-angle scattering study of such alloys has not yet been performed.

For the ferromagnetic concentration range of the ED Ni-P alloys which was studied here for $11 \lesssim x \lesssim 15$, it was found that the behavior of the matrix magnetization can be reasonably well described with the Stoner-Edwards-Wohlfarth theory[24] of very weak itinerant ferromagnetism and the concentration dependence of $\sigma(0,0)$ and T_c followed the theory of Mathon,[27] which was also derived within the framework of the SEW model. This behavior corresponds to expectation in that starting at high P contents with a Pauli paramagnetic Ni-P phase (no exchange splitting of the d subbands, i.e., $T_c = 0$) and, by decreasing the P content, we should arrive, beyond a critical concentration, at a situation where a small exchange splitting (small, but finite T_c) of the d subbands is induced. Since the d bands at these concentrations are, although not yet completely but still to a large extent filled, the difference of the spin-up and spin-down d-band populations (or holes), i.e., the net magnetization, is very small and these are just the conditions for VWIF. This could, indeed, be observed here immediately beyond the PM-FM transition due to the fairly low amount of magnetic inhomogeneities in our ED Ni-P alloys (if a large amount of strongly magnetic inhomogeneities were present, the PM-FM transition would proceed via percolation, i.e., through the gradual strengthening of the coupling between the magnetic polarization clouds). However, since the Arrott plots and Mathon plots were found to describe our data well down to $x = 11.5$ and for $x \lesssim 13$ the saturation magnetization $\sigma(0,0)$ exceeded already about 10 emu/g, at the lower end of the concentration range studied here the condition of VWIF ($\zeta \ll 1$) is no longer fulfilled and the alloys here behave as WIF. Since pure fcc Ni behaves like a SIF, we should expect another transition (WIF$\rightarrow$SIF) with decreasing P content below 11.5 at. %. Although the satu-

ration magnetization and T_c have already been measured[2] for ED Ni-P alloys below 10 at. % P, a more detailed magnetization study would be necessary to observe this transition. These data would also facilitate an evaluation of the composition dependence of the electronic structure of Ni-P alloys on which results of low-temperature electronic specific heat measurements[46,49,55] and theoretical band-structure calculations[47] are already also available.

ACKNOWLEDGMENTS

One of the authors (I.B.) is indebted to G. Dietz for useful discussions and correspondence. This work was partially supported by the OTKA Board of Hungary through Grant No. 2942. The Cu substrate foils used for the electrodeposition were kindly donated by the Csepel Metal Works, Budapest. Financial support was also provided by the Soros Foundation, Hungary.

*Deceased.

[1]J. Crangle and M. J. C. Martin, Philos. Mag. **4**, 1006 (1959).

[2]P. A. Albert, Z. Kovac, H. R. Lilienthal, T. R. McGuire, and Y. Nakamura, J. Appl. Phys. **38**, 1258 (1967).

[3]R. J. Gambino, T. R. McGuire, and Y. Nakamura, J. Appl. Phys. **38**, 1253 (1967).

[4]D. Pan and D. Turnbull, in *Magnetism and Magnetic Materials—1973 (Boston),* Proceedings of the 19th Annual Conference on Magnetism and Magnetic Materials, edited by C. D. Graham, Jr. and J. J. Rhyne, AIP Conf. Proc. No. 18 (AIP, New York, 1974), p. 646.

[5]A. Berrada, M. F. Lapierre, B. Loegel, P. Panissod, and C. Robert, J. Phys. F **8**, 845 (1978).

[6]K. Hüller, G. Dietz, R. Hausmann, and K. Kölpin, J. Magn. Magn. Mater. **53**, 103 (1985).

[7]I. Bakonyi, L. K. Varga, A. Lovas, E. Tóth-Kádár, and A. Sólyom, J. Magn. Magn. Mater. **50**, 111 (1985).

[8]R. Sonnberger, E. Pfanner, and G. Dietz, Z. Phys. B **63**, 203 (1986).

[9]A. Amamou, F. Gautier, and B. Loegel, J. Phys. F **5**, 1342 (1975).

[10]A. Amamou and J. Durand, Commun. Phys. **1**, 191 (1976).

[11]U. Pittermann and S. Ripper, Phys. Status Solidi A **93**, 131 (1986).

[12]G. Dietz, T. Laska, H. D. Schneider, and F. Stein, J. Less-Common Met. **145**, 573 (1988).

[13]S. N. Kaul and M. Rosenberg, Phys. Rev. B **25**, 5863 (1982).

[14]I. Bakonyi, P. Panissod, and R. Hasegawa, J. Appl. Phys. **53**, 7771 (1982).

[15]E. Tóth-Kádár, I. Bakonyi, A. Sólyom, J. Hering, G. Konczos, and F. Pavlyák, Surf. Coat. Technol. **31**, 31 (1987).

[16]E. Tóth-Kádár, I. Bakonyi, J. Lóránth, A. Sólyom, L. Pogány, T. Dankházi, J. Tóth, G. Konczos, P. Fodor, and H. H. Liebermann, Plat. Surf. Fin. **77** (9), 70 (1990).

[17]L. Varga, K. Tompa, and T. Schmidt, Phys. Status Solidi A **68**, 603 (1981).

[18]H. Maeda, Jpn. J. Appl. Phys. **8**, 978 (1969).

[19]J. Tóth, I. Bakonyi, and H. H. Liebermann, in *Digest (F) of the International Conference Low Temperature Physics Budapest 87* (Central Research Institute for Physics, Budapest, 1987), p. 61.

[20]I. Bakonyi, H. Ebert, W. Socher, J. Voitländer, E. Wachtel, N. Willmann, and B. Predel, J. Magn. Magn. Mater. **68**, 47 (1987).

[21]E. Wachtel, I. Bakonyi, J. Bahle, N. Willmann, A. Lovas, A. Burgstaller, W. Socher, J. Voitländer, and H. H. Liebermann, Mater. Sci. Eng. A **133**, 196 (1991).

[22]W. A. Hines, C. U. Modzelewski, R. N. Paolino, and R. Hasegawa, Solid State Commun. **39**, 699 (1981).

[23]G. Dietz and H. D. Schneider, J. Phys. Condens. Matter **2**, 2169 (1990).

[24]D. M. Edwards and E. P. Wohlfarth, Proc. R. Soc. London, Ser. A **303**, 127 (1968).

[25]S. Ogawa and N. Sakamoto, J. Phys. Soc. Jpn. **22**, 1214 (1967); S. Foner, E. J. McNiff, Jr., and V. Sadagopan, Phys. Rev. Lett. **19**, 1233 (1967); G. S. Knapp, F. Y. Fradin, and H. V. Culbert, J. Appl. Phys. **42**, 1341 (1971).

[26]K. P. Belov and A. N. Goryaga, Fiz. Met. Metalloved. **2**, 3 (1956); A. Arrott, Phys. Rev. **108**, 1394 (1957); J. S. Kouvel (unpublished), cited in Ref. 24.

[27]J. Mathon, Proc. R. Soc. London, Ser. A **306**, 355 (1968).

[28]H. L. Alberts, J. Beille, D. Bloch, and E. P. Wohlfarth, Phys. Rev. B **9**, 2233 (1974).

[29]E. P. Wohlfarth, J. Phys. (Paris) Colloq. **32**, C1-636 (1971).

[30]S. Shtrikman and E. P. Wohlfarth, Physica **60**, 427 (1972).

[31]A. Berrada, Thèse de 3me cycle, Université Louis L. Pasteur, Strasbourg, 1976.

[32]F. Acker and R. Huguenin, J. Magn. Magn. Mater. **12**, 58 (1979).

[33]K. K. Murata and S. Doniach, Phys. Rev. Lett. **29**, 285 (1972).

[34]T. Moriya and A. Kawabata, J. Phys. Soc. Jpn. **34**, 639 (1973); **35**, 669 (1973); *Spin-fluctuations in Itinerant Electron Magnetism,* edited by T. Moriya (Springer, Berlin, 1985).

[35]A. Lienard and J. P. Rebouillat, J. Appl. Phys. **49**, 1680 (1978); A. Lienard, J. P. Rebouillat, P. Garoche, and J. J. Veyssié, J. Phys. (Paris) Colloq. **41**, C8-658 (1980).

[36]H. Yamada and E. P. Wohlfarth, Phys. Status Solidi B **58**, K151 (1973); **64**, K71 (1974); Phys. Lett. **51A**, 65 (1975).

[37]E. P. Wohlfarth, Phys. Lett. **69A**, 222 (1978); D. Wagner and E. P. Wohlfarth, J. Phys. F **9**, 717 (1979); J. Magn. Magn. Mater. **15-18**, 1345 (1980).

[38]I. S. Jacobs and C. P. Bean, in *Magnetism,* edited by G. T. Rado and H. Suhl (Academic, New York, 1963), Vol. III, Chap. 6.

[39]E. Kneller, in *Ferromagnetismus,* edited by H. P. J. Wijn, Handbuch der Physik Vol. XVIII/2 (Springer-Verlag, Berlin, 1966), p. 438.

[40]T. Furubayashi and I. Nakatani, Solid State Commun. **74**, 821 (1990).

[41]T. Moriya, Physica B **86-88**, 356 (1977).

[42]E. P. Wohlfarth, J. Magn. Magn. Mater. **7**, 113 (1978).

[43]O. M. Tolkachev and N. I. Yurasov, J. Phys. Condens. Matter **3**, 2947 (1991).

[44]A. Amamou, D. Aliaga Guerra, P. Panissod, G. Krill, and R. Kuentzler, J. Phys. (Paris) Colloq. **41**, C8-396 (1980).

[45]M. Goto, H. Tange, T. Tokunaga, H. Fujii, and T. Okamoto, Jpn. J. Appl. Phys. **16**, 2175 (1977).

[46]R. Kuentzler, I. Bakonyi, and A. Lovas, Solid State Commun. **55**, 567 (1985); U. Mizutani and I. Bakonyi, J. Phys. F **16**, 1583 (1986).

[47]W. Y. Ching, Phys. Rev. B **34**, 2080 (1986); S. S. Jaswal, *ibid.* **34**, 8937 (1986); M. R. Press, S. N. Khanna, and P. Jena, *ibid.*

36, 5446 (1987); Hyungjin Yang, J. C. Swihart, D. M. Nicholson, and R. H. Brown, Phys. Rev. B **47**, 107 (1993).

[48]P. H. Gaskell, J. Non-Cryst. Solids **32**, 207 (1979); P. H. Gaskell, in *Glassy Metals II,* edited by H.-J. Güntherodt and H. Beck, Topics in Applied Physics Vol. 53 (Springer-Verlag, Berlin, 1983), p. 5.

[49]P. J. Cote, G. P. Capsimalis, and G. L. Salinger, in *Amorphous Magnetism II,* edited by R. A. Levy and R. Hasegawa (Plenum, New York, 1977), p. 499.

[50]A. W. Simpson and D. R. Brambley, Phys. Status Solidi B **49**, 685 (1972).

[51]K. Iida, J. Magn. Magn. Mater. **35**, 226 (1983).

[52]T. Osaka, M. Usuda, I. Koiwa, and H. Sawai, Jpn. J. Appl. Phys. **27**, 1885 (1988).

[53]J. R. Nelson, L. E. Toth, and J. H. Judy, J. Electron. Mater. **7**, 123 (1978).

[54]K. Schild, F. Frisius, P. Lamparter, and S. Steeb, Z. Naturforsch., Teil A **40**, 551 (1985).

[55]Y. S. Tyan and L. E. Toth, J. Electron. Mater. **3**, 791 (1974).